SAND2017-13192C

Denoising 400-kHz "Postage-Stamp PIV" using Uncertainty Quantification

Steven J. Beresh[1]
Sandia National Laboratories, Albuquerque, NM, 87185

A new approach to denoising Time-Resolved Particle Image Velocimetry data is proposed by incorporating measurement uncertainties estimated using the correlation statistics method. The denoising algorithm of Oxlade et al (*Experiments in Fluids*, 2012) has been modified to add the frequency dependence of PIV noise by obtaining it from the uncertainty estimates, including the correlated term between velocity and uncertainty that is zero only if white noise is assumed. Although the present approach was only partially effective in denoising the 400-kHz "postage-stamp PIV" data, important and novel insights were obtained into the behavior of PIV uncertainty. The belief that PIV noise is white noise has been shown to be inaccurate, though it may serve as a reasonable approximation for measurements with a high dynamic range. Noise spectra take a similar shape to the velocity spectra because increased velocity fluctuations correspond to higher shear and therefore increased uncertainty. Coherence functions show that correlation between velocity fluctuations and uncertainty is strongest at low and mid frequencies, tapering to a much weaker correlation at high frequencies where turbulent scales are small with lower shear magnitudes.

Introduction

The measurement of turbulent velocity spectra in high-speed flows has been an instrumentation challenge for decades. In large part, this is because of the very high frequencies that must be reached at small spatial scales to capture the transfer of turbulent energy from the larger production scales towards dissipation scales. If detection of the onset of the inertial subrange is a goal for such measurements, Pope predicts this to occur at frequencies of about 40-100 kHz in flows of current interest to Sandia [1]. Unfortunately, the most common means of measuring velocity spectra fail to reach such frequency response. Hot-wire anemometry has been widely used but recent studies indicate that limitations in spatial resolution restrict the frequency response to much lower values, apparently in the 5-20 kHz range [2, 3]. The clear exception is the nano-scale thermal anemometry probe, which in fact can achieve a frequency response exceeding 150 kHz [4, 5]. Laser Doppler velocimetry has been widely used for high-speed turbulence measurements as well, but fast acquisition rates lie only in the 10-20 kHz range and the accuracy of high-frequency content is limited by the non-uniform particle arrival rate [6, 7]. Both techniques also may have difficulties collecting all three velocity components simultaneously without interference between them or differing spatial sampling parameters. Emerging techniques based upon the Doppler shift of the laser light itself show promise for reaching much faster sampling rates, but have not yet achieved more than limited application [8, 9].

In contrast, time-resolved particle image velocimetry (TR-PIV) has rapidly found widespread use in low-speed flows and recently has been demonstrated in a high-speed wind tunnel using a pulse-burst laser [10], which is the only light source capable of producing sufficient energy at the necessarily rapid pulse rates. Temporal phenomena were measured by pulse-burst PIV to repetition rates reaching 50 kHz and are key to understanding the dominant physics describing the behavior of high-speed flows. However, the turbulent behavior at all but the largest scales occurs at still higher frequencies. More advanced algorithms are available that can move spatial information into time to extract

[1]Distinguished Member of the Technical Staff, Engineering Sciences Center, AIAA Associate Fellow, correspondence to: P.O. Box 5800, Mailstop 0825, (505) 844-4618, email: sjberes@sandia.gov

considerably higher frequencies from TR-PIV than would be indicated by the framing rate [11-13], but these require assumptions whose validity is limited in many flows of interest.

Given these limitations, a need exists for still faster implementations of TR-PIV. PIV has been demonstrated at 1 MHz by Wernet and Opalski [14] and Brock et al [15] but these were limited to sequences of 7 and 13 vector fields, respectively, which is inadequate to obtain spectral content. In contrast, Beresh et al [16] modified their pulse-burst PIV system to reach very high frequencies by greatly reducing the field of view. The laser energy available at high frequencies is considerably reduced and must be confined to a smaller area if sufficient scattered energy is to be collected. Current high-speed camera technology allows very fast image acquisition for long time sequences if the field of view is windowed down to a small array. Combining these approaches, pulse-burst PIV was acquired at 400 kHz for image sequences exceeding 4,000 frames, but by necessity for a small array of only 128 × 120 pixels, giving rise to the moniker of "postage-stamp PIV." Despite the limited spatial extent, this approach was shown to be well-suited to measuring turbulent velocity spectra without the use of any frozen turbulence assumptions.

Still, the postage-stamp PIV of Beresh et al [16] reached frequency limitations of approximately 100-150 kHz due to interference from the noise floor of the measurement. Some impact of the noise may have distorted the measured spectra at lower frequencies, particularly in a stereoscopic implementation. To accurately measure the highest frequencies that can be delivered by postage-stamp PIV and detect the turbulent phenomena that motivate the technique, a noise reduction scheme is necessary. The need for such denoising algorithms has been evident in low-speed applications of TR-PIV, but the approaches that have been developed [17-19] are difficult to implement in the present case. Either an assumed spectral form is required [18] or an accurate estimate of the noise floor must be produced from oversampled data [19], neither of which is suitable to the high-speed flows for which postage-stamp PIV is intended. Moreover, the algorithms are predicated on an assumption that PIV noise is white noise [17, 19], which will be shown herein not to be the case.

Meanwhile, capabilities for uncertainty quantification of PIV measurements have matured dramatically in recent years, with several methods having been implemented [20-23]. These allow each individual vector in PIV to be given its own unique uncertainty estimate, as opposed to a general estimate applied identically across the data set as was common for most of PIV's history. Each of the four methods has its merits, but the most accurate uncertainty estimates have been shown to result from Wieneke's method [24, 25], which has the additional advantage of being readily available in commercial software.

The noise in PIV ultimately results from the error in each individual vector, and the uncertainty quantification method of Wieneke [23] allows a reasonable estimate to be made of that error and hence the noise present in the overall data set. In principle, the uncertainties calculated for the PIV data set then could be used to quantify the characteristics of the noise that seep into the velocity spectra and therefore could form the basis for a new denoising algorithm for TR-PIV. Previously, Wieneke [26] has demonstrated that uncertainty characteristics can be used to remove noise from vector fields, but his technique functions entirely on a spatial basis and does not recognize the temporal content that gives rise to the spectral noise under consideration here. A new perspective that considers the temporal properties of PIV uncertainty would overcome the limitations of previous denoising algorithms in application to postage-stamp PIV, thereby increasing the effective frequency response of the measurement and the accuracy of the spectra at high frequencies. The present paper will explore a new approach to denoising TR-PIV data based upon the concepts of Oxlade et al [19] but incorporating the actual uncertainties of the measurement as provided by Wieneke's method [23].

Experimental Configuration

A brief description of postage-stamp PIV is provided here, with the full details to be found in Beresh et al [16].

The development of postage-stamp PIV has been performed using a supersonic jet exhausting into a transonic crossflow, identically to previous efforts [10, 16]. This work was conducted in Sandia's Trisonic Wind Tunnel (TWT), which is a blowdown-to-atmosphere facility using air as the test gas through a test section of dimensions 305 × 305 mm^2 (12 × 12 $inch^2$). Mach 0.8 was tested exclusively for the data used herein at a fixed stagnation pressure of 154 kPa and stagnation temperature of 321K ± 2K. A supersonic jet was installed on the top wall of the test section upstream of the windows, as seen in Fig. 1a, for measurement of the far-field of the jet interaction. A nitrogen jet exhausted from a conical nozzle with a design Mach number of 3.73, an expansion half-angle of 15 deg, and an exit diameter of 9.53 mm. In the present case, the jet was operated at a pressure of 3.9 MPa to produce a jet-to-freestream dynamic pressure ratio of J=8.1. The laser sheet was introduced through a window in the floor of the test section and was aligned to the streamwise center plane of the test section, which coincides with the center of the jet nozzle exit. The coordinate axes originate at the centerpoint of the nozzle exit plane; the u component is in the streamwise direction and v component is positive away from the top wall of the tunnel.

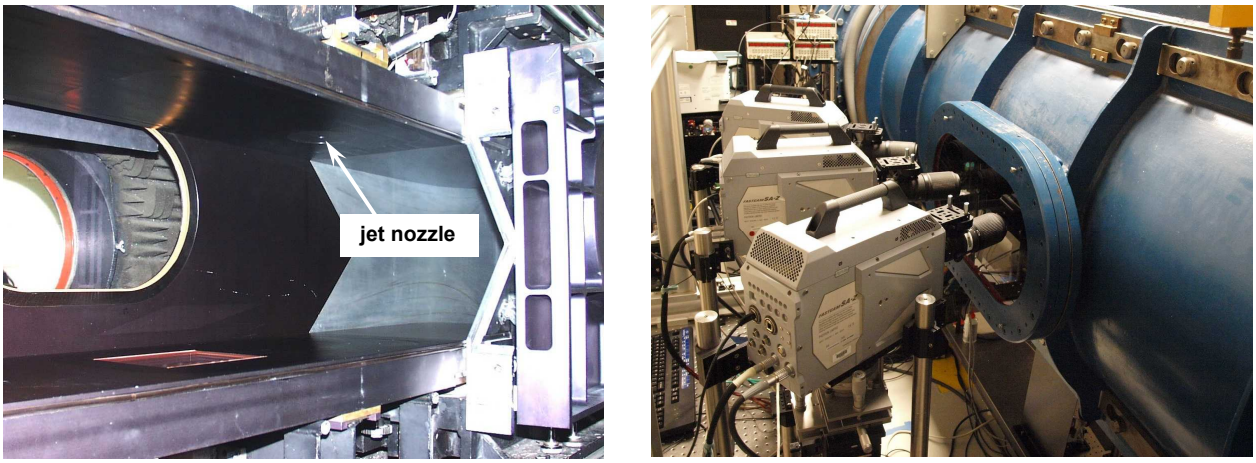

(a) **(b)**

Fig. 1: Photo of the experimental configurations. (a) The jet-in-crossflow experiment. (b) The camera setup for the postage-stamp PIV.

The TWT is seeded by a thermal smoke generator (Corona Vi-Count 5000) whose output is delivered to the TWT's stagnation chamber upstream of the flow conditioning section. Previous measurement of the in-situ particle response across a shock wave generated by a wedge reveal a frequency response of 500-700 kHz, corresponding to a particle size of 0.7 - 0.8 μm when sphericity is assumed. Stokes numbers have been estimated as at most 0.05 based on *a posteriori* analysis of PIV measurements, which is sufficiently small to render particle lag errors negligible.

A burst-mode laser (QuasiModo-1000, Spectral Energies, LLC) with both diode- and flashlamp-pumped Nd:YAG amplifiers was used to produce a high-energy pulse train at 532 nm. The pulse-burst laser generates a burst of maximum duration 10.2 ms once every 8 seconds with a maximum repetition rate of 500 kHz. For postage-stamp PIV, it was operated to deliver single pulses at 400 kHz with an energy of about 8 mJ per pulse at 532 nm, creating a time between successive pulses of 2.5 μs. The laser sheet was narrowed to a slender width to concentrate the available energy in the small field of view and had a sheet thickness of 1 mm. A total of about 170 bursts of data were acquired.

Images were acquired using high-speed CMOS cameras (Photron SA-Z) which have an array of 1024 × 1024 pixels at a full framing rate of 20 kHz. Their windowing function allows the framing rate to be increased by sampling a semi-arbitrary portion of the imaging array. The SA-Z cameras were operated at 400 kHz, which necessitates that they are windowed down to a small array of only 128 × 120 pixels; hence the use of the term "postage-stamp PIV."

Three SA-Z cameras were used to acquire two independent measurements, as seen in Fig. 1b. One camera was aligned for a conventional two-component measurement. The other two cameras combined for a stereoscopic measurement with each camera oriented at a half-angle of 20 deg. The cameras each were equipped with 200-mm focal length lenses and anti-peak-locking diffuser plates [27]. Scheimpflug mounts were used to ensure focus of the two oblique images. Calibration details are found in [16]. The two-component configuration provides a safe measurement without possibility of bias due to an inadequate calibration with such a small field of view, but a successful stereo measurement offers three-component data for evaluation of the turbulent kinetic energy spectra.

Data were processed using LaVision's DaVis v8.3.1. In each case, image pairs were background corrected, intensity normalized, and then interrogated with an initial pass using 64 × 64 pixel interrogation windows, followed by two iterations of Gaussian-weighted 24 × 24 pixel interrogation windows. A 50% overlap in the interrogation windows was used as well. The resulting vector fields were validated based upon signal-to-noise ratio, nearest-neighbor comparisons, allowable velocity range, and a median filter in both space and time.

Summary of Experimental Results

The field of view for the postage-stamp PIV is shown in Fig. 2. The full extent of the jet-in-crossflow experiment is given in Fig. 2a using conventional 10-Hz PIV [28], with the vertical component of the mean velocity field shown positioned in its far-field location. Superposed are the fields of view for both the 25-kHz pulse-burst PIV described in [10] and the postage-stamp PIV [16]. Figure 2b reproduces a previous pulse-burst PIV vector field from [10] as well as the postage-stamp PIV field of view. The small size of the postage-stamp PIV window is evident, little more

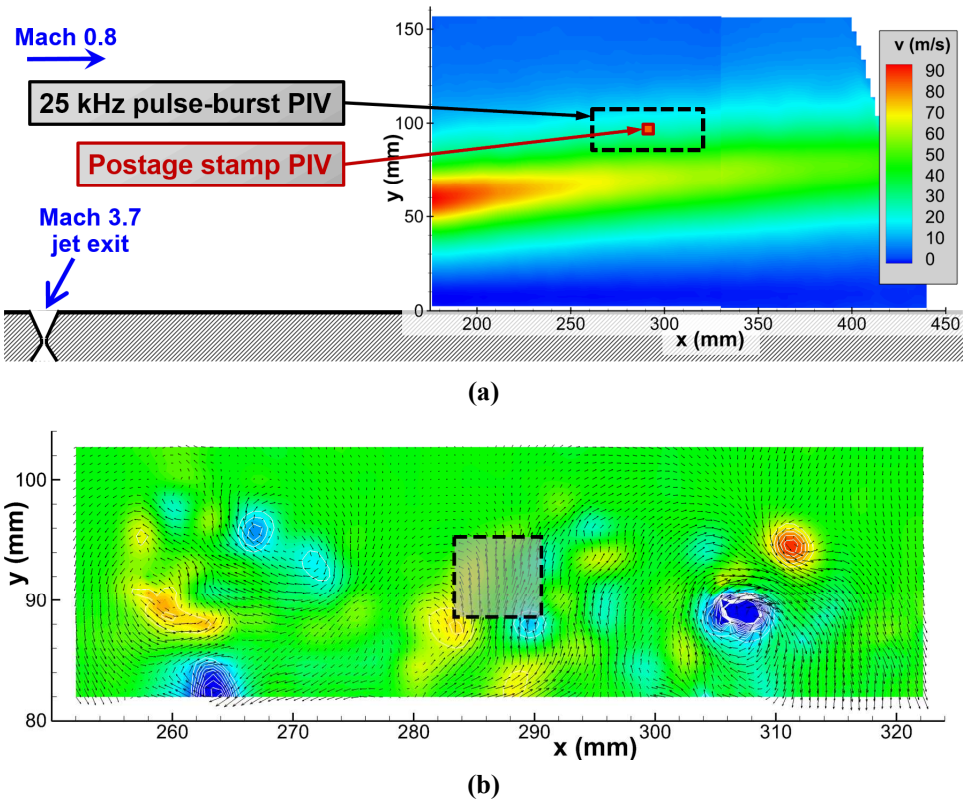

Fig. 2: Field of view of the postage-stamp PIV measurement within the larger jet-in-crossflow experiment superposed on: (a) a conventional PIV mean vector field of the far-field [27], and (b) a snapshot from the earlier 25-kHz pulse-burst PIV data [10].

than a point measurement. This measurement will reveal little about the structure of the flow given its minimal extent, but this is a necessary sacrifice to achieve the very high framing rate that can yield high-frequency spectral content.

Upgrades to the laser system since the previous postage-stamp PIV measurements [16] have allowed acquisition of lower-noise data by improving the beam profile and pointing stability. These enhancements reduce correlation noise, but do not represent a sufficiently large enhancement as to obviate the need for a denoising algorithm. Nonetheless, data presented here represent an improvement from the previously reported data set [16] but employ an identical experimental configuration.

The power spectra of the velocity fluctuations that are measured by the two-component postage-stamp PIV are shown in Fig. 3. Two PSD plots are shown, one for the streamwise component of velocity fluctuations and the other for the vertical component. In the present case, the properties of the jet interaction change very little within the far-downstream field of view and it suffices to examine the spectra at a single point near the center of the field of view where no edge effects interfere with computing correlations as particles may exit the field of view. Slopes for -1 and -5/3 power law dependencies are provided as well. Also shown are spectra for the uncertainty estimates, which will be described subsequently.

For both velocity components in Fig. 3, the spectral content of the flow is visible to high frequencies until the noise floor intrudes at about 120 kHz. The most consequential of the spectra is the vertical component in Fig. 3b. The spectra peak at 4 kHz, which corresponds to one full period between pairs of turbulent eddies convecting through the flow [29]. Following the peak, the spectra then exhibit a -1 slope dependence to about 60-70 kHz before gradually transitioning to an apparent -5/3 slope dependence. The presence of the -5/3 region is well-known and expected as a consequence of the inertial subrange of turbulence decay (e.g., Pope [1]). The -1 dependence, on the other hand, is an unanticipated discovery and lasts for at least one full decade, from approximately 4 – 60 kHz. It is discussed in more detail in [16].

The streamwise component in Fig. 3a also appears to be supportive of a -1 slope dependence but its lack of a peak means this region does not initiate until about 8 kHz. The -5/3 slope dependence at high frequencies is somewhat less

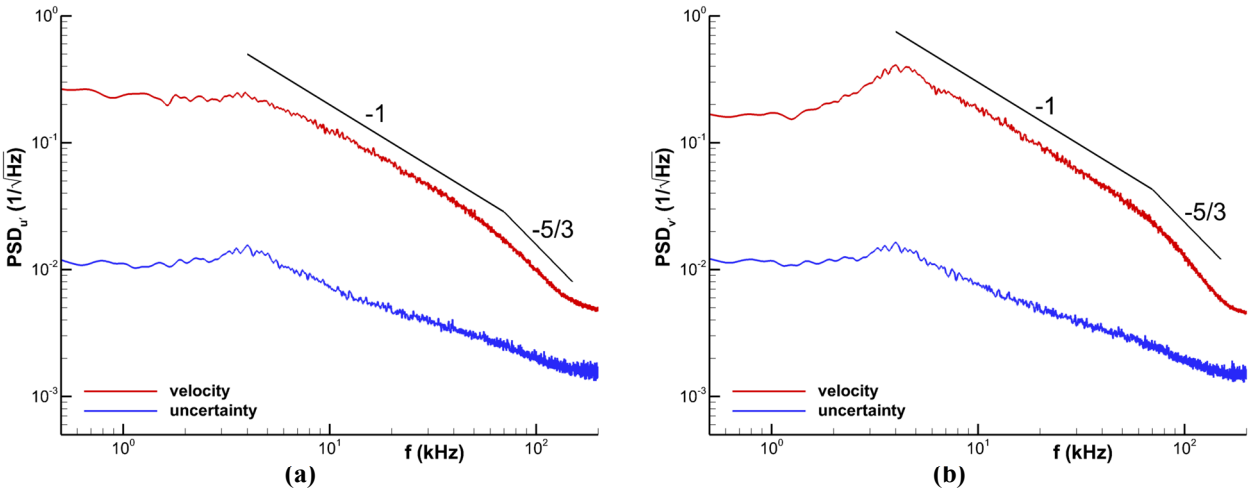

Fig. 3: Postage-stamp PIV power spectra of velocity fluctuations for the jet in crossflow. Spectra from uncertainty estimates also are shown. (a) streamwise component; (b) vertical component.

convincing for the streamwise component than for the vertical component. This is because the overall intensity of the streamwise velocity fluctuations is reduced compared to the vertical velocity fluctuations, and therefore the impact of the noise floor is felt sooner.

The stereoscopic postage-stamp PIV measurements offer turbulent kinetic energy spectra rather than the one-dimensional spectra examined in Fig. 3. This is important because turbulent theory typically is based upon three-dimensional fluctuations rather than one-dimensional. Figure 4 shows one-dimensional spectra for each of the three components of the stereo measurement. The two in-plane components appear similar to their two-component counterparts in Fig. 3, but a closer comparison reveals deviations. Although the noise floor is similar in both cases, the power-law slope is different in the inertial subrange for the stereo data as compared to the two-component measurement, and its onset is earlier. This difference in slope in the inertial subrange is attributable to poorer spatial resolution in the stereo measurement because of the oblique camera images and the registration of two cameras, which increases the practical size of each interrogation window and thereby lowers the associated frequency response.

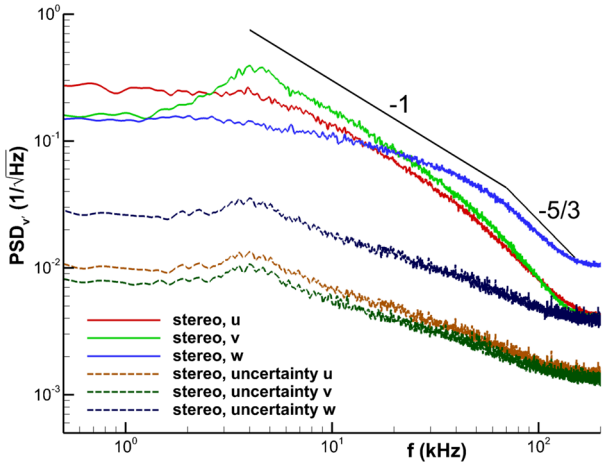

Fig. 4: Power spectra of each of the three components of the stereoscopic postage-stamp PIV as well as the corresponding uncertainty estimates.

The spectrum of the out-of-plane component, *w*, exhibits a considerably higher noise floor than the two in-plane components, *u* and *v*. Moreover, values are elevated at mid-range frequencies as well, which is likely inaccurate as *w* fluctuations should not be more intense than *u* or *v* fluctuations in this frequency band alone. The elevated noise in the *w* component of the stereo measurements can be attributed to the propagation of precision uncertainties from the two constituent correlations into in-plane and out-of-plane components. Classical analyses predict that for the present camera angles (about a 20-deg half-angle), the precision uncertainty in the out-of-plane component *w* is approximately 2-3 times greater than the in-plane component *u* [30, 31]. A recent, more sophisticated analysis is agreeable [32]. These estimates would be consistent with the noise floor differences in Fig. 4, for which the *w* floor has magnitude of 0.013 and the *u* floor is .006, or a ratio of 2.2. Uncertainty estimation drawn from the actual postage-stamp PIV images using the correlation statistics method [23] indeed shows that the uncertainty in the *w* component is consistently about 2.3 times greater than that in the *u* component. The intensity of the *w* spectrum remains elevated above the *v* spectrum in the range of 30-100 kHz by about 0.010 to 0.018, which suggests that this effect constitutes additive noise of a magnitude consistent with the noise floor. The *v* and *w* components should be most similar because both are

induced by the counter-rotating vortex pair. Taken together, these observations suggest that the aberrant nature of the *w* component is a result of increased correlation noise in the out-of-plane component of stereo PIV.

The clear presence of increased noise in the *w* component and its apparent distortion of the spectrum suggests that the lower noise levels in *u* and *v* may plausibly alter those spectra as well, though to a lesser extent. These effects are likely to become significant at frequencies greater than the approximately 30 kHz at which the *w* component begins to express deviance, but it is unclear how much greater. Therefore, the development of a denoising algorithm for postage-stamp PIV is necessary.

Evaluating the Oxlade et al Denoising Algorithm

The most well developed denoising algorithm for TR-PIV probably is that of Oxlade et al [19], who proceeded to test it in low-speed grid turbulence against a hot-wire anemometer. They define the measured variance of the velocity $\hat{u}$ as the sum of actual variance of the flow u, the variance of the error in the measurement ε, and a correlation term between the two, as follows:

$$\langle \hat{u}_i^2 \rangle = \langle u_i^2 \rangle + \langle \varepsilon_i^2 \rangle + 2R_{u_i\varepsilon_i}\sigma_{u_i}\sigma_{\varepsilon_i} \quad (1)$$

In this notation, the subscript *i* represents each component of velocity and its associated uncertainty.

At this point, they assert that random error in PIV is white noise, which follows models instituted by Vetel et al [17] and Foucaut et al [33]. This allows two simplifications important to their algorithm. First, the correlation coefficient in the third term on the right-hand side of equation 1 becomes identically zero and that term may be eliminated. Secondly, since their data are oversampled in a low-speed flow, at high frequencies the noise floor is well distinguished from any residual signal. This permits a sample of the noise at high frequencies to be applied across the spectrum.

Oxlade et al then transform equation 1 into spectral integrals:

$$\int \widehat{\Phi}_{u_i}(f)df = \int \left[\Phi_{u_i}(f) + \Phi_{\varepsilon_i}(f)\right]df \quad (2)$$

If PIV is indeed white noise, then the noise floor has no frequency dependence and equation 2 becomes:

$$\Phi_{u_i}(f) = \widehat{\Phi}_{u_i}(f) - \Phi_{\varepsilon_i} \quad (3)$$

The noise floor then may be obtained from high frequencies where the noise dominates the signal and applied across the spectrum to create a denoising filter. An accurate estimate of the noise floor generally demands that the noise greatly exceeds the signal at a frequency about four times larger than the smallest measured turbulent event [19]. As is evident in Fig. 3, the present postage-stamp PIV measurement does not reach a sufficiently large frequency for the noise floor to fully discriminate itself from the desired signal. In low-speed applications of TR-PIV, oversampled data is common and hence this requirement is achievable.

Therefore, the formulation in Eq. 3 is predicated on an assumption of white noise, both to simplify the denoising process into something tractable and to obtain a noise sample from the high-frequency region of oversampled data. This critical assumption may be evaluated using recent developments in uncertainty quantification for PIV. Rather than estimating random error in PIV based on a high-frequency sample, an estimate of that error instead may be obtained more directly using uncertainty quantification. To this purpose, Wieneke's correlation statistics method [23] was applied to the entire postage-stamp PIV dataset. Since this provides a unique uncertainty estimate for each individual vector, a time sequence of uncertainties is inherently created and this may be transformed into a spectrum just as a velocity time sequence.

The spectra of uncertainty estimates are included in Figs. 3 and 4. Several interesting observations may be made about the character of the uncertainty spectra. First, clearly they are not white noise. A strong correlation with the magnitude of the velocity fluctuations is seen. At frequencies where energy in u_i' is elevated, the uncertainty magnitude ε_i is elevated as well. In fact, the shape of the uncertainty spectra looks remarkably like that of the corresponding velocity spectra, including an apparent constant power-law region in the uncertainty corresponding to the region of -1 slope that has been identified for the velocity spectra. Where higher noise is found for the out-of-plane component of the stereoscopic measurements, the uncertainty is correspondingly raised as well. It also is noteworthy that the uncertainty spectra for the *u* and *w* components in Figs. 3a and 4 retain the 4-kHz peak that is found in the *v* component of velocity but not the *u* and *w* velocity components. This is important because shear in one component is known to increase the uncertainty in all velocity components due to its effect on the correlation peak [20-23].

The behavior of the uncertainty spectra is consistent with the collection of recently developed uncertainty quantification techniques [20-23], all of which note that increased velocity gradients correspond to increased uncertainty. Though this observation strictly applies to spatial gradients in velocity and u_i' is due to a temporal gradient, in turbulent flows temporal and spatial velocity gradients can be expected to be strongly correlated. Figure 5 demonstrates that the present measurements exhibit a strong correlation between velocity fluctuation and uncertainty

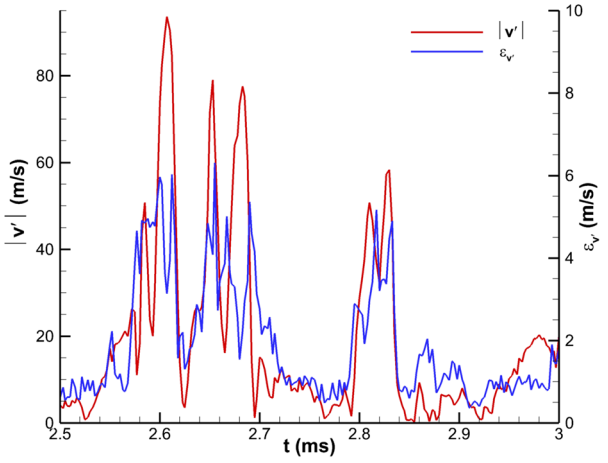

Fig. 5: Sample time history of the absolute value of the vertical velocity fluctuations and the corresponding uncertainty estimate.

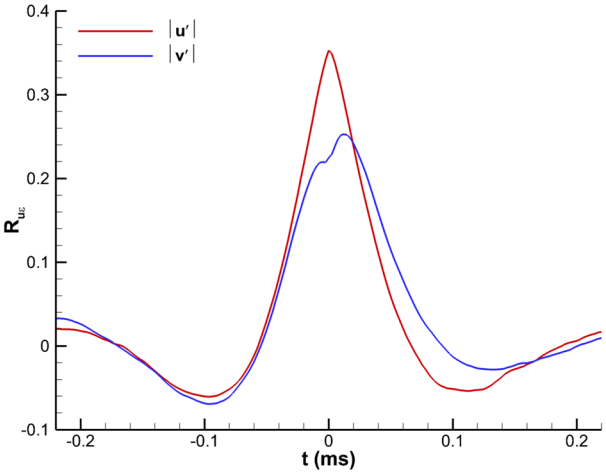

Fig. 6: Cross-correlation of the absolute value of each velocity component with the uncertainty estimate.

by displaying a sample time history of v' along with the corresponding ε_v. Where the absolute value of v' is large, ε_v also is large; analogously, low values in each parameter are found simultaneously as well. This is clearer in Fig. 6, which shows the cross-correlation function between velocity and uncertainty for both u and v components; clearly, values of $R_{u\varepsilon}$ from Eq. 1 are significant. The correlation between velocity fluctuations and uncertainty is a result of moments of higher turbulent shear increasing the magnitude of both parameters.

From the established evidence found in [20-23] combined with the present data as exemplified by Figs. 5 and 6, an argument follows that random error in PIV cannot be white noise. This is experimentally demonstrated by the uncertainty spectra included in Figs. 3 and 4.

Modifying the Oxlade et al Denoising Algorithm

If the uncertainty quantification method of Wieneke [23] provides reasonable estimates of the spectra of PIV noise, can it be used to denoise the velocity data? This could be accomplished by returning to equation 1 with the recognition that $R_{u\varepsilon} \neq 0$ and proceeding to derive a new denoising formula. Equation 2 then becomes:

$$\int \widehat{\Phi}_{u_i}(f)df = \int \Phi_{u_i}(f)\,df + \int \Phi_{\varepsilon_i}(f)\,df + 2R_{u_i\varepsilon_i}\sigma_{u_i}\sigma_{\varepsilon_i} \tag{4}$$

The additional term on the right can be determined directly from the postage-stamp PIV data and its associated uncertainty values. The second term on the right, which previously was simplified by using an assumption of white noise, now may be replaced with the noise spectrum provided by the uncertainty quantification methodology. This should provide all necessary content to denoise the data, without resorting to the erroneous assumption of white noise for PIV random error. The final term on the right should be a function of frequency, which yields:

$$\int \widehat{\Phi}_{u_i}(f)df = \int \Phi_{u_i}(f)\,df + \int \Phi_{\varepsilon_i}(f)\,df + 2\int \sigma_{u_i}(f)\sigma_{\varepsilon_i}(f)R_{u_i\varepsilon_i}(f)df \tag{5}$$

And now the final term on the right may be recognized as the cross-spectrum of u_i and ε_i, denoted as $\gamma_{u\varepsilon}$, also known as the coherence function $C_{u\varepsilon}$ if normalized. This creates:

$$\int \widehat{\Phi}_{u_i}(f)df = \int \Phi_{u_i}(f)\,df + \int \Phi_{\varepsilon_i}(f)\,df + 2\int \gamma_{u_i\varepsilon_i}(f)df \tag{6}$$

Since the integrands on each side must be equal:

$$\widehat{\Phi}_{u_i}(f) = \Phi_{u_i}(f) + \Phi_{\varepsilon_i}(f) + 2\gamma_{u_i\varepsilon_i}(f) \tag{7}$$

Again adapting the approach of Oxlade et al [19], who rewrite equation 3 as:

$$\Phi_{u_i}(f) = \widehat{\Phi}_{u_i}(f)\,H_i(f) \tag{8}$$

From this, they write a transfer function $H_i(f)$ as:

$$H_i(f) = 1 - \frac{\Phi_{\varepsilon_i}}{\widehat{\Phi}_{u_i}(f)} \tag{9}$$

The present analysis suggests that if equation 9 is corrected such that white noise is no longer assumed, the transfer function becomes:

$$H_i(f) = 1 - \frac{\Phi_{\varepsilon_i}(f)}{\widehat{\Phi}_{u_i}(f)} - \frac{2\gamma_{u_i\varepsilon_i}(f)}{\widehat{\Phi}_{u_i}(f)} \tag{10}$$

All parameters in equation 10 can be found from the postage-stamp PIV data and the associated uncertainty quantification. At that point, the denoising algorithm of Oxlade et al [19] may be resumed using the modified transfer function.

Three different transfer functions may be calculated. In the original Oxlade et al formulation, Eq. 9 is used and $\Phi_{\varepsilon i}$ is considered to be white noise and therefore has no frequency dependence; this is denoted $H_i(white)$. Alternatively, the same equation may be used but $\Phi_{\varepsilon i}$ redefined to include frequency dependence; this is $H_i(Oxlade)$. Finally, the modified denoising algorithm uses Eq. 10 and is named $H_i(modified)$. The latter two formulations of H_i allow assessment of the impact of the correlated term independent of the white noise approximation.

Figure 7 shows these three transfer functions as well as the coherence function that results from the cross-spectrum of u_i and ε_i. $H_i(white)$ uses the Oxlade et al approach, in which the noise is assumed to be white noise and the value is determined where the noise floor emerges at high frequencies. This already is known to be ineffective in the present case because the signal cannot be oversampled for such a high-speed flow, and therefore the noise floor does not adequately separate from the signal. Nonetheless, an estimate of the noise magnitude is extracted from the frequency range 180 – 200 kHz and used to create a transfer function. As it must, $H_i(white)$ trends to zero at the highest measurable frequency, which means the corrected signal also must trend to zero. This cannot be correct as the present goal is to remove the noise and leave behind the remaining signal. In Oxlade et al, the oversampled signal trends to zero at high frequencies and therefore it is proper for $H_i(white)$ to do so as well. This transfer function is included only to demonstrate that it is unsuitable to present needs.

The Oxlade et al transfer function may be expanded to incorporate noise variable with frequency. The frequency-dependent noise is obtained from the spectra of uncertainty found in Fig. 3. This yields the $H_i(Oxlade)$ transfer function in Fig. 7. As can be seen, this has the advantage of not trending towards zero at high frequencies and therefore would leave some signal behind after denoising. In addition, some small degree of noise would be removed at lower frequencies, but this still exceeds the amount removed due to the white noise estimate. This effect follows naturally from the spectra of uncertainty in Fig. 3, which show higher uncertainty magnitudes at lower frequencies than in the high-frequency limit.

Finally, the modified transfer function given by $H_i(modified)$ shows high-frequency behavior quite similar to the $H_i(Oxlade)$ transfer function but considerably more energy is removed at lower frequencies with greater dependency upon the frequency. This can be understood by examining the coherence functions, which also are included in Fig. 7. These define the relative magnitude of the correlated term in Eq. 10 and therefore its distribution with respect to frequency. Though the shape varies a little for the two velocity components, the coherence magnitude is considerably greater at low and mid frequencies than it is at high frequencies. Therefore the effect of the correlated term on the transfer function is small at high frequencies and little distinguishes $H_i(modified)$ from $H_i(Oxlade)$ in this range. It is physically credible that coherence is greatest at low to mid frequencies and very small at high frequencies. Shear will be greatest at mid to large flow scales and therefore coherence between velocity fluctuations and uncertainty will be largest at such frequencies. Smaller measurable scales will have smaller shear magnitudes and therefore a smaller impact on uncertainty, leading to low coherence at high frequencies.

The transfer functions of Fig. 7 are used to denoise the velocity spectra, the results of which are shown in Fig. 8. The white noise transfer function clearly destroys the signal at high frequencies and cannot be correct for non-oversampled data as in the present case. The difference between the effects of $H_i(modified)$ and $H_i(Oxlade)$ at high frequencies is minimal because the correlated term is so small as evidenced by the coherence functions in Fig. 7. Some loss of signal is created by $H_i(modified)$ at low and mid frequencies because the correlated term is significant in those frequency ranges. But the key observation from Fig. 8 is that the denoising using the modified Oxlade et al algorithm is only minimally effective. At high frequencies, some noise is removed but a roll-off to a reduced noise floor is still evident. In fact, the modified approach is scarcely more effective than simply banishing the white noise approximation in the Oxlade transfer function, which is because the correlated term is so small at high frequencies. Either way, the denoising correction is only partially effective and much noise still remains in the signal even after application.

The use of $H_i(modified)$ leaves two difficulties in its performance. First, while the correlated term may be mathematically sound at all frequencies, the relatively large coherence leads to a significant subtraction of energy at low frequencies that appears unjustified. Experiments that have compared TR-PIV spectra to hot-wire spectra have not observed notable discrepancies at low to mid frequencies [19, 24] and therefore no such correction ought to be expected. Second, because the uncertainty magnitude tapers off at high frequency and the correlated term is nearly negligible, too little noise is removed from the signal at precisely those frequencies at which it is most contaminating the measurement. A substantial noise floor remains even after denoising, and hence the current denoising algorithm still does not capture all of or even most of the noise that is present.

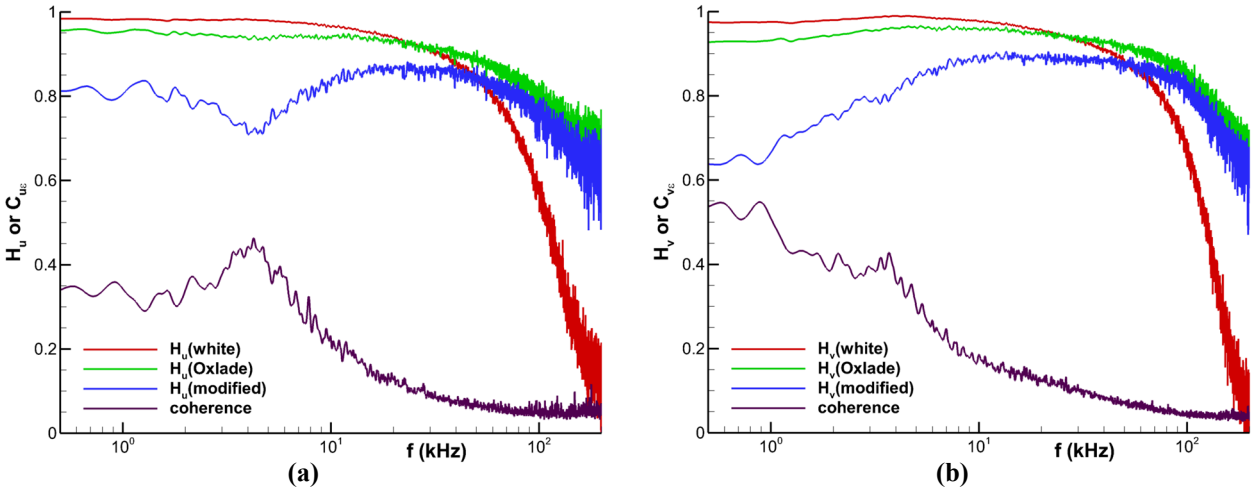

Fig. 7: Coherence function of velocity to uncertainty and denoising transfer functions. (a) streamwise component; (b) vertical component.

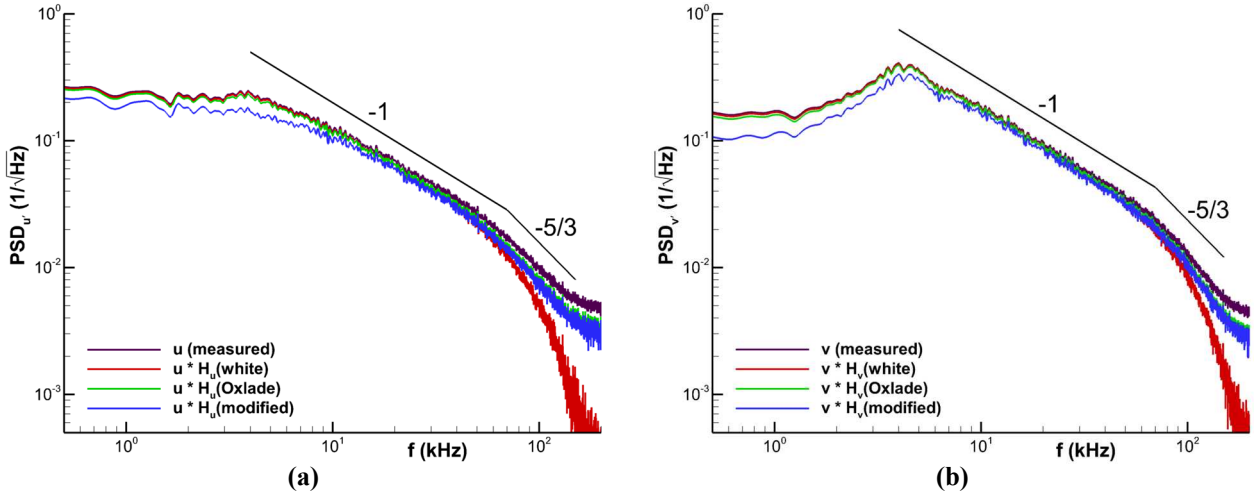

Fig. 8: Denoised power spectra using the transfer functions of Fig. 7. (a) streamwise component; (b) vertical component.

On a related note, it is likely that Oxlade et al's approximation of white noise is tolerable for their application in a low-speed flow with high turbulence levels, in which the dynamic range between signal levels and noise levels often exceeds two orders of magnitude. This means deviations from the white noise approximation still are small fractions of the total measured signal. Conversely, the present postage-stamp PIV data demonstrate signal-to-noise ratios of no more than 1.5 orders of magnitude and often less, and the noise levels are a more significant portion of the measured signal. Therefore, an accurate denoising algorithm cannot successfully proceed using a white noise approximation and instead must be based upon the true spectral distribution of the noise.

Finally, the related concept of Wieneke's spatial denoising algorithm that is similarly based upon uncertainty quantification [26] has been tested and does not reduce the noise floor in the spectrum. This experience validates the need to employ an algorithm based upon temporal content.

An Alternative Approach Based upon Adaptive Filtering

A common means of removing noise from temporal measurements is use of an adaptive filter. This essentially is a digital implementation of an optimal filter (or Wiener filter), in which a feedback loop is used to adjust filter coefficients until the common portion of two input signals is returned. Sensors are spaced far enough apart that their signals are statistically identical but their valid data is uncorrelated, whereas a common noise source remains correlated. Thus the correlated portion of the two signals found by the adaptive filter approximates the noise and can

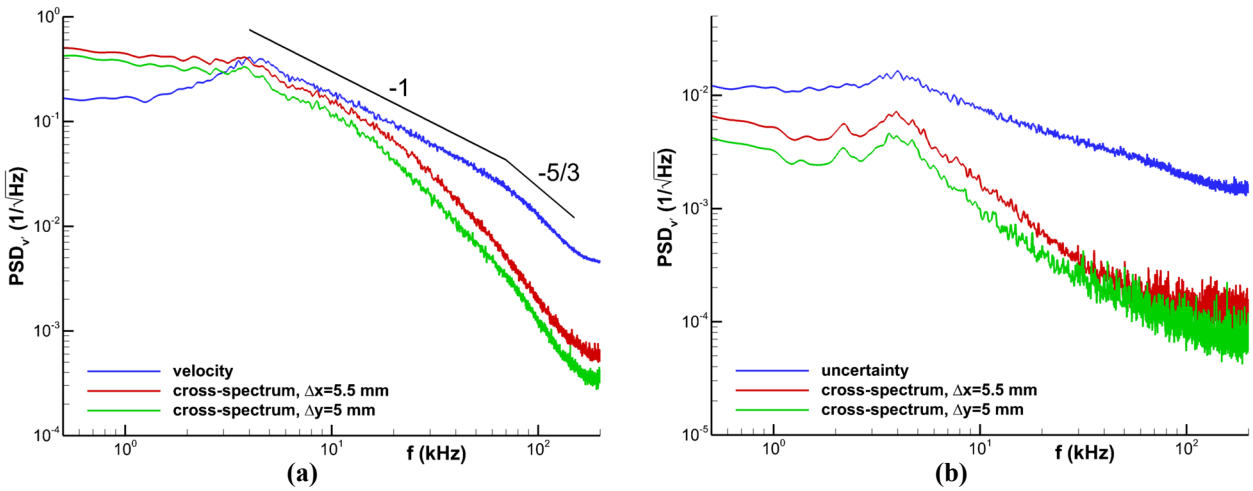

Fig. 9: Cross-spectrum of two points spanning the postage-stamp PIV field of view. (a) vertical velocity component; (b) uncertainty of vertical velocity component.

be subtracted from the signal to produce a noise-canceled signal. Such an approach has been successfully used to cancel wind tunnel noise from turbulent pressure fluctuation data [34] using an adaptive filtering scheme much like that of Naguib et al [35].

Vetel et al also used an optimal filter to denoise TR-PIV data, but their operation was performed at a single spatial point by relying upon the white noise approximation to describe PIV noise [17]. Oxlade et al determined that use of the optimal filter biased low the resulting spectral energy in the denoised signal [19].

In the present case, the troublesome noise source occurs at high frequencies. The useful signal due to turbulent fluctuations at these frequencies is expected to cover small spatial scales given the relationship between wavenumber and frequency in turbulence. Even for the tiny field of view of the present 400-kHz "postage-stamp PIV," a single PIV measurement covers a sufficiently large extent as to separate vectors at the edges of the field by a greater distance than that associated with high-frequency turbulence. If the high-frequency noise source were correlated over longer scales than the high-frequency turbulence, then it may be treatable using an adaptive filter analogous to that used in pressure fluctuation data.

To assess this possibility, cross-spectrum densities were computed for two points in the flow. This was performed twice, once spanning the maximum distance in the horizontal direction ($\Delta x \approx 5.5$ mm) and again for the maximum distance in the vertical direction ($\Delta y \approx 5$ mm). These results are given in Fig. 9a. Here, only the vertical velocity component is shown because the streamwise component performs similarly and therefore including it does not provide additional insight. The absence of correlation at the highest measurable frequencies demonstrates that turbulent features generating these velocity fluctuations do not extend over the two-point separation. Since the noise floor of the cross-spectrum plots falls an order of magnitude below that of the velocity PSD, this indicates that the high-frequency noise does not correlate over such distances.

The lack of spatial correlation of high-frequency noise can be confirmed by performing similar cross-spectrum analysis of the uncertainty estimates for the same two-point separations as Fig. 9a. These are given in Fig. 9b and compared to the spectrum of the uncertainty from Fig. 3b. Again, at high frequencies the correlated energy falls well below that of the single-point PSD, indicating that the high-frequency noise does not correlate over even the small extent of the postage-stamp PIV. This emphasizes the earlier observation that local shear is one of the dominant drivers of PIV uncertainty and that the frequency content associated with the source of that shear is also found in the uncertainty. Therefore, the concept of employing an adaptive filter to denoise TR-PIV data at high frequencies appears not to be viable.

Conclusions and Future Work

A new approach to denoising Time-Resolved Particle Image Velocimetry data is proposed by incorporating measurement uncertainties estimated using the correlation statistics method. The denoising algorithm of Oxlade et al [19] has been modified to include the frequency dependence of PIV noise by obtaining it from the uncertainty estimates, including the correlated term between velocity and uncertainty that is zero only if white noise is assumed.

Even though the present modification to the Oxlade et al denoising algorithm was only partially effective in denoising the 400-kHz "postage-stamp PIV" data, a number of important and novel insights were obtained into the behavior of PIV uncertainty. The belief that PIV noise is white noise has been shown to be inaccurate, though it may serve as a reasonable approximation for measurements with a high dynamic range. Inclusion of the frequency dependence of uncertainty is necessary to obtain a mathematically correct implementation of noise effects. Spectra of the uncertainty take a similar shape to the matching velocity spectra because increased velocity fluctuations correspond to higher shear and therefore increased uncertainty. This previously has been demonstrated spatially and now is confirmed spectrally. Coherence functions show that correlation between velocity fluctuations and uncertainty is strongest at low and mid frequencies, tapering to a much weaker correlation at high frequencies where turbulent scales are small with lower shear magnitudes. High-frequency noise is locally determined and cannot be isolated by two-point correlations.

Further development of the denoising technique is planned. Application to the low-speed data set of Neal et al [24] is underway and may be more suitable to assessing the technique due to its oversampled nature, its superior dynamic range, and matching hot-wire data. Alternative means of making use of the spatial content from adjacent vectors also is contemplated but presently immature.

References

[1] Pope, S. B., *Turbulent Flows,* Cambridge University Press, 2000, pp. 228-242.

[2] Ashok, A., Bailey, S. C. C., Hultmark, M., and Smits, A. J., "Hot-Wire Spatial Resolution Effects in Measurements of Grid-Generated Turbulence," *Experiments in Fluids*, Vol. 53, No. 6, 2012, pp. 1713-1722.

[3] Hutchins, N., Monty, J. P., Hultmark, M., and Smits, A. J., "A Direct Measure of the Frequency Response of Hot-Wire Anemometers: Temporal Resolution Issues in Wall-Bounded Turbulence," *Experiments in Fluids*, Vol. 56, No. 1, 2015, pp. 18.

[4] Bailey, S. C. C., Kunkel, G. J., Hultmark, M., Vallikivi, M., Hill, J. P., Meyer, K. A., Tsay, C., Arnold, C. B., and Smits, A. J., "Turbulence Measurements using a Nanoscale Thermal Anemometry Probe," *Journal of Fluid Mechanics*, Vol. 663, 2010, pp. 160-179.

[5] Vallikivi, M., Hultmark, M., Bailey, S. C. C., and Smits, A. J., "Turbulence Measurements in Pipe Flow using a Nano-Scale Thermal Anemometry Probe," *Experiments in Fluids*, Vol. 51, No. 6, 2011, pp. 1521-1527.

[6] Benedict, L. H., Nobach, H., and Tropea, C., "Edtimation of Turbulent Velocity Spectra from Laser Doppler Data," *Measurement Science and Technology*, Vol. 11, No. 8, 2000, pp. 1089-1104.

[7] Broersen, P. M. T., "Practical Aspects of the Spectral Analysis of Irregularly Sampled Data with Time-Series Models," *IEEE Transactions on Instrumentation and Measurement*, Vol. 58, No. 5, 2009, pp. 1380-1388.

[8] Strand, O. T., Goosman, D. R., Martinez, C., Whitworth, T. L., and Kuhlow, W. W., "Compact System for High-Speed Velocimetry using Heterodyne Techniques," *Review of Scientific Instruments*, Vol. 77, No. 8, 2006, pp. 083108.

[9] Ecker, T., Brooks, D. R., Lowe, K. T., and Ng, W. F., "Development and Application of a Point Doppler Velocimeter Featuring Two-Beam Multiplexing for Time-Resolved Measurements of High-Speed Flow," *Experiments in Fluids*, Vol. 55, No. 3, 2014, pp. 1819.

[10] Beresh, S. J., Kearney, S. P., Wagner, J. L., Guildenbecher, D. R., Henfling, J. F., Spillers, R. W., Pruett, B. O. M., Jiang, N., Slipchenko, M., Mance, J., and Roy, S., "Pulse-Burst PIV in a High-Speed Wind Tunnel," *Measurement Science and Technology*, Vol. 26, No. 9, 2015, pp. 095305.

[11] Scarano, F., and Moore, P., "An Advection-Based Model to Increase the Temporal Resolution of PIV Time Series," Experiments *in Fluids,* Vol. 52, No. 4, 2012, pp. 919-933.

[12] Schneiders, J. F. G., Dwight, R. P., and Scarano, F., "Time-Supersampling of 3D-PIV Measurements with Vortex-in-Cell Simulation," *Experiments in Fluids*, Vol. 55, No. 3, 2014, pp. 1692.

[13] Schreyer, A.-M., Larchevêque, L., and Dupont, P., "Method for Spectra Estimation from High-Speed Experimental Data," *AIAA Journal*, Vol. 54, No. 2, 2016, pp. 557-568.

[14] Wernet, M. P., and Opalski, A. B., "Development and Application of a MHz Frame Rate Digital Particle Image Velocimetry System," AIAA Paper 2004-2184, June 2004.

[15] Brock, B., Haynes, R. H., Thurow, B. S., Lyons, G., and Murray, N. E., "An Examination of MHz Rate PIV in a Heated Supersonic Jet," AIAA Paper 2014-1102, January 2014.

[16] Beresh, S. J., Henfling, J. F., and Spillers, R. W., "Postage-Stamp PIV: Small Velocity Fields at 400 kHz for Turbulence Spectra Measurements," AIAA Paper 2017-0024, January 2017.

[17] Vetel, J., Garon, A., and Pelletier, D., "Denoising Methods for Time-Resolved PIV Measurements," *Experiments in Fluids*, Vol. 51, No. 4, 2011, pp. 893-916.

[18] Gamba, M., and Clemens, N. T., "Requirements, Capabilities and Accuracy of Time-Resolved PIV in Turbulent Reacting Flows," AIAA Paper 2011-0362, January 2011.

[19] Oxlade, A. R., Valente, P. C., Ganapathisubramani, B., and Morrison, J. F., "Denoising of Time-Resolved PIV for Accurate Measurement of Turbulence Spectra and Reduced Error in Derivatives," *Experiments in Fluids*, Vol. 53, No. 5, 2012, pp. 1561-1575.

[20] Timmins, B. H., Wilson, B. W., Smith, B. L., and Vlachos, P. P., "A Method for Automatic Estimation of Instantaneous Local Uncertainty in Particle Image Velocimetry Measurements," *Experiments in Fluids*, Vol. 53, No. 4, 2012, pp. 1133-1147.
[21] Charanko, J. J., and Vlachos, P. P., "Estimation of Uncertainty Bounds for Individual Particle Image Velocimetry Measurements from Cross-Correlation Peak Ratio," *Measurement Science and Technology*, Vol. 24, No. 6, 2013, 065301.
[22] Sciacchitano, A., Wieneke, B., and Scarano, F., "PIV Uncertainty Quantification by Image Matching," *Measurement Science and* Technology, Vol. 24, No. 4, 2013, 045302.
[23] Wieneke, B., "PIV Uncertainty Quantification from Correlation Statistics," *Measurement Science and Technology*, Vol. 26, No. 7, 2015, pp. 074002.
[24] Neal, D. R., Sciacchitano, A., Smith, B. L., and Scarano, F., "Collaborative Framework for PIV Uncertainty Quantification: The Experimental Database," *Measurement Science and Technology*, Vol. 26, No. 7, 2015, pp. 074003.
[25] Sciacchitano, A., Neal, D. R., Smith, B. L., Warner, S. O., Vlachos, P. P., Wieneke, B., and Scarano, F., "Collaborative Framework for PIV Uncertainty Quantification: Comparative Assessment Methods," *Measurement Science and Technology*, Vol. 26, No. 7, 2015, pp. 074004.
[26] Wieneke, B., "PIV Anisotropic Denoising using Uncertainty Quantification," *Experiments in Fluids*, Vol. 58, No. 8, 2017, p. 94.
[27] Michaelis, D., Neal, D. R., and Wieneke, B., "Peak-Locking Reduction for Particle Image Velocimetry," *Measurement Science and Technology*, Vol. 27, No. 10, 2016, pp. 104005.
[28] Beresh, S. J., Henfling, J. F., Erven, R. J., and Spillers, R. W., "Penetration of a Transverse Supersonic Jet into a Subsonic Compressible Crossflow," *AIAA Journal*, Vol. 43, No. 2, 2005, pp. 379-389.
[29] Beresh, S. J., Wagner, J. L., Henfling, J. F., Spillers, R. W., and Pruett, B. O. M., "Turbulent Eddies in a Compressible Jet in Crossflow Measured using Pulse-Burst Particle Image Velocimetry," *Physics of Fluids*, Vol. 28, No. 2, 2016, pp. 025102
[30] Zang, W., and Prasad, A. K., "Performance Evaluation of a Scheimpflug Stereocamera for Particle Image Velocimetry," *Applied Optics*, Vol. 36, No. 33, 1997, pp. 8738-8744.
[31] Lawson, N. J., and Wu, J., "Three-Dimensional Particle Image Velocimetry: Error Analysis of Stereoscopic Techniques," *Measurement Science and Technology*, Vol. 8, No. 8, 1997, pp. 894-900.
[32] Bhattacharya, S., Charanko, J. J., and Vlachos, P. P., "Stereo-Particle Image Velocimetry Uncertainty Quantification," *Measurement Science and Technology*, Vol. 28, No. 1, 2017, pp. 015301.
[33] Foucaut, J. M., Carlier, J., and Stanislas, M., "PIV Optimization for the Study of Turbulent Flow using Spectral Analysis," *Measurement Science and Technology*, Vol. 15, No. 4, 2004, pp. 1046-1058.
[34] Beresh, S. J., Henfling, J. F., Spillers, R. W., and Pruett, B. O. M., "Fluctuating Wall Pressures Measured Beneath a Supersonic Turbulent Boundary Layer," *Physics of Fluids*, Vol. 23, No. 7, 2011, pp. 075110.
[35] Naguib, A. M., Gravante, S. P., and Wark, C. E., "Extraction of Turbulent Wall-Pressure Time-Series using an Optimal Filtering Scheme," *Experiments in Fluids*, Vol. 22, No. 1, 1996, pp. 14-22.